Stability of the peroxide group in BaO₂ under high pressure

Xinyu Zhang,^{1,2,3} Xiaoshan Luo,^{1,2} Maxim Bykov,^{3,4} Elena Bykova,³ Irina Chuvashova,^{3,5} Denys Butenko,⁶ Stella Chariton,⁷ Vitali Prakapenka,⁷ Dean Smith,⁸ Hongbo Wang,¹ Yanchao Wang,^{1,2} Jian Lv,^{1,2,*} and Alexander F. Goncharov,^{3,†}

¹State Key Laboratory of Superhard Materials, College of Physics, Jilin University, Changchun 130012, China
²International Center for Computational Method and Software, College of Physics, Jilin University, Changchun 130012, China
³Earth and Planets Laboratory, Carnegie Institution of Washington, Washington, DC 20015, USA
⁴Department of Mathematics, Howard University, Washington, DC 20059, USA
⁵Harvard Physics, Jefferson Physical Lab, 17 Oxford Street, Cambridge, Massachusetts 02138, USA
⁶Sino-Russian International Joint Laboratory for Clean Energy and Energy Conversion Technology, College of Physics,
International Center of Future Science, Jilin University, Changchun 130012, China
⁷Center for Advanced Radiation Sources, University of Chicago, Chicago, Illinois 60637, USA
⁸HPCAT, X-ray Science Division, Argonne National Laboratory, Lemont, Illinois 60439, USA

10

12

13

16

17

19

20

21

23

25

26

30

31

33

34

36

37

39

42

(Received 23 September 2020; revised 9 February 2021; accepted 10 February 2021; published xxxxxxxxxx)

Alkaline earth metal peroxides are typical examples of ionic compounds containing polyanions. We herein report a stable BaO_2 phase at high pressure up to 130 GPa found via a first-principles computational structure search and high-pressure experimental investigations. The identified monoclinic structure (space group C2/m) can be derived by sublattice distortions of Ba atoms and peroxide groups associated with the phonon mode softening of the lower-pressure Cmmm structure. Contrary to the previous expectation of polymerization of the peroxide group at elevated pressure, this phase retains the peroxide group and, interestingly, exhibits an insulating behavior demonstrating an increase of the band gap under compression. Our synchrotron x-ray diffraction (XRD) measurements could not distinguish between Cmmm and C2/m BaO₂ definitively because the difference in XRD patterns is very subtle. However, our data do not show any sign of polymerization transition up to 120 GPa. Raman spectra of the O-O peroxide vibration show a small anomaly in frequency at 110 GPa, which is qualitatively like that predicted theoretically due to the Cmmm to C2/m phase transition, thus supporting the predicted transformation.

DOI: 10.1103/PhysRevB.00.004100

I. INTRODUCTION

Alkaline earth metal peroxides ($M^{\rm II}{\rm O}_2$ with $M^{\rm II}={\rm Be, Mg, Ca, Sr, Ba}$) are typical examples of ionic compounds containing polyanions, in which the peroxide [O-O]²⁻ group is bound by a single O-O bond, and each O atom attracts one electron from the metal atom in accordance with the octet rule [1,2]. Because of the remarkable reactivity and oxidant capacity, they have long been used in widely diversified areas of industry and agriculture [3–5]; for example, barium peroxide is an exceptionally strong oxidizing agent in pyrotechnics, bleaching, and energy storage [6–8].

Much effort has been made to uncover the structures and properties of $M^{II}O_2$ compounds under various external conditions for both basic scientific interests and practical applications. There was an early structural report on alkaline earth metal [9], but only BaO₂ and SrO₂ have been synthesized in pure form thus far [10]. It has been found that, although the metal cations belong to the same group of the periodic table, the resulting peroxides exhibit very different

behaviors. Generally, the stabilities of $M^{II}O_2$ increase as the metal goes down the Group II. Indeed, beryllium peroxide BeO₂ is unlikely to exist, while MgO₂ with pyrite structure (space group Pa-3) is metastable at ambient conditions, and it can be readily decomposed upon heating [11,12]. A recent high-pressure experiment synthesized magnesium peroxide MgO₂ at pressure above 96 GPa and 2150 K [13]. This form of MgO₂ has the I4/mcm structure and may exist in the depth of rocky planets [13]. Heavier alkaline earth metals Ca, Sr, and Ba form peroxides with increasing stabilities, all of which were assigned to a CaC₂-type structure with the space group of I4/mcm at ambient conditions based on early x-ray diffraction (XRD) experiments [9,12,14,15]. However, the determination of the O positions is a great challenge for XRD measurements due to a very small scattering cross-section. Recent theoretical studies based on global structure prediction methods proposed ground-state structures for both CaO₂ and SrO₂ that are more energetically favorable than the CaC₂-type structure [12,16,17]. Meanwhile, the rich pressure-induced polymorphism of CaO₂ and SrO₂ has been proposed [16,17].

As a heavy member of the $M^{II}O_2$ group, the high-pressure behavior of BaO₂ is relatively less explored. Only recent experiment revealed a pressure-induced reversible structural

51

60

63

66

69

70

^{*}lvjian@jlu.edu.cn

[†]agoncharov@carnegiescience.edu

135

137

138

140

141

143

144

146

147

149

150

153

155

158

159

160

161

162

163

165

168

171

172

175

177

178

182

183

185

186

74

77

80

82

85

100

101

102

104

105

106

107

110

111

112

113

114

115

116

117

118

119

120

121

122

124

125

128

transformation from the CaC₂-type structure to an orthorhombic *Cmmm* structure near 33 GPa, which is closely related to the NaCl-to-CsCl-type transformations common for ionic AB compounds under pressure [15]. Considering the rich high-pressure phases of CaO₂ and SrO₂, it is of interest to explore the high-pressure behaviors of BaO₂, which is crucial for a systematic understanding of the alkaline earth metal peroxides, including the pressure-induced transitions of CaC₂-type structures.

In this paper, we report a high-pressure behavior of BaO₂ based on ab initio global structure search calculations and high-pressure experiments. Our structure search uncovered a monoclinic phase of BaO₂ with space group C2/m to be stable at pressure above \sim 110 GPa. Unlike the previous conjecture that high pressure may induce a polymerization of O₂ units in BaO₂, leading to an AlB₂-type structure with graphene-like O sheets [15], the C2/m phase preserves the peroxide O_2 groups, which show an out-of-plane distortion following the softening of the phonon mode in the lower-pressure Cmmm phase. The high-pressure XRD pattern of BaO₂ up to 130 GPa can be indexed with the monoclinic C2/m as well as lowerpressure Cmmm phases, while the Raman frequency of the stretching peroxide mode shows a subtle anomaly supporting the theoretically predicted phase transition. The detailed structural description is given, and the transition mechanism is discussed.

II. COMPUTATIONAL AND EXPERIMENTAL DETAILS

The search for high-pressure structures of the BaO_2 compound was performed by the swarm-intelligence-based CALYPSO method [18–21]. The key feature of this methodology is its capability of predicting the ground-state stable structure of materials with only the knowledge of chemical composition at given external conditions (for example, pressure), not relying on any prior known structural information. Its validity has been manifested by successful identification of the ground-state structures for many systems [22–26].

The underlying energy calculations and structure optimizations were performed in the framework of density functional theory (DFT) using the Vienna ab initio Simulation Package [27]. The projector-augmented plane-wave [28] approach was used to represent the ion-electron interaction with $5s^25p^66s^2$ and $2s^22p^4$ valence electrons for Ba and O, respectively. The electron exchange-correlation functional was treated using the generalized gradient approximation proposed by Perdew, Burke, and Ernzerhof [29]. The cutoff radius of the pseudopotentials of oxygen and hydrogen were 0.58 and 0.42 Å, respectively. A cutoff energy of 850 eV for the expansion of the wave function into plane-waves and appropriate regular Monkhorst-Pack k-point grids of $2\pi \times 0.03 \,\text{Å}^{-1}$ were chosen to ensure that all enthalpy calculations were well converged to 1 meV/atom. Phonon calculations were carried out using the frozen phonon approach as implemented in the PHONOPY package [30]. The Visualization for Electronic and Structural Analysis software (VESTA 3) was used for visualization and plotting [31].

Diamond anvils with culets of 300- and 60- μ m diameter beveled to 300 μ m were used to access the 0–40 and 0–30 GPa pressure range, respectively. Rhenium foils were

laser drilled to create cavities (30 μ m in diameter) serving as sample chambers. BaO₂ polycrystalline powder (Millipore Sigma, ≥86%) was loaded in the sample chambers with no pressure medium under nitrogen atmosphere to avoid reactions with moisture and carbon dioxide from the air. Synchrotron XRD measurements were used in situ at high pressure in the diamond anvil cells to determine the onset of chemical and physical transformations. These were performed at the undulator beamlines 13ID-D GSECARS and 16ID-B HPCAT of APS (ANL) using the x-ray beam (wavelengths $\lambda = 0.2952$ and 0.4066 A, respectively) focused to approximately 4 μ m spot size. The offline double-sided laser-heating system of HPCAT was used for laser heating at the highest pressure reached of 130 GPa. Synchrotron XRD was collected in situ at high pressure in the diamond anvil cells to determine the onset of chemical and physical transformations. Twodimensional XRD patterns were integrated using the DIOPTAS software [32]. Raman characterization of the sample was performed with solid-state laser lines of 532 and 632.8 nm as excitation sources, which were focused to the spots of 3-4 and $\sim 5 \mu m$ in diameter, respectively. The Raman spectra of BaO₂ were measured concomitantly with XRD using the offline Raman system at GSECARS [33] and in a separate experiment at Jilin university. The pressure was estimated by the position of the stressed diamond Raman edge [34], which was found to show inconsistent results in concomitant XRD-Raman experiments for the sample volume, and the Raman frequency on the pressure increased and decreased. Thus, we used the pressure dependence of the O-O stretching mode determined in Jilin experiment to determine pressure in XRD experiments.

III. RESULTS AND DISCUSSION

Structure searching calculations were performed at 0, 50, 100 and 150 GPa, respectively. Both the previous CaC₂-type and orthorhombic Cmmm structures of BaO2 were well reproduced by our calculations at 0 and 50 GPa, respectively, validating our methodology in application to dense Ba-O systems. The tetragonal CaC2-type structure with two formula units per unit cell (space group I4/mmm, Z=2) can be described as a distorted NaCl-type structure, with Ba atoms on the Na site, and the centers of O₂ dumbbells occupying the Cl site. All peroxide units are parallel to the c axis pointing to the Ba atoms. Both the Ba atoms and O2 dumbbells are six coordinated with respect to each other, forming elongated octahedra [Fig. 1(a)]. The orthorhombic Cmmm structure (Z = 2) can be described as a distorted CsCl archetype, in which Ba atoms and O₂ dumbbells form distorted cubes and are eightfold coordinated to each other. The O2 dumbbells are aligned parallel to the b axis and form pseudohexagonal graphenelike sheets [Fig. 1(b)]. It is speculated that, under significant high pressure (e.g., above 100 GPa), O₂ dumbbells in Cmmm structure may polymerize to graphenelike layers, leading to an AlB₂-type structure with the metallic properties [15].

In addition to the previous known structures, our structure searches at 100 and 150 GPa uncovered a monoclinic C2/m structure with four formula units per unit cell [Fig. 1(c)]. The structural parameters of this structure at 150 GPa are a =

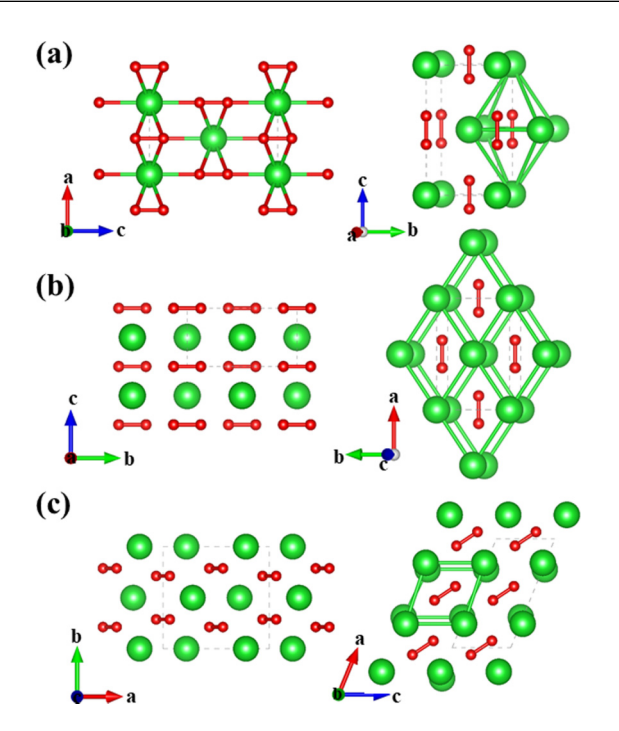


FIG. 1. Crystal structures of various BaO_2 phases: (a) the tetragonal CaC_2 -type I4/mmm structure, (b) the orthorhombic Cmmm structure, and (c) the monoclinic C2/m structure. The large (green) and small (red) spheres correspond to Ba and O atoms, respectively.

6.382 Å, b = 5.689 Å, c = 3.190 Å, and $\beta = 112.112^{\circ}$ with Ba on 4 i (0.280, 0, 0.039) and O on 8 j (0.064, 0.213, 0.370) sites. Within this structure, the peroxide O_2 units remain without signs of polymerization, and they still lie in parallel to each other. The structure features eightfold coordination of the peroxide groups and Ba atoms. Compared with the orthorhombic *Cmmm* structure, O_2 dumbbells exhibit large out-of-plane angular distortions, leading to highly wrinkled O layers.

Figure 2(a) shows the calculated static enthalpies for the four phases of BaO_2 . The tetragonal CaC_2 -type structure is stable up to about 33 GPa, beyond which the orthorhombic *Cmmm* structures are energetically more favored. The transition pressure is in good agreement with the previous experiment measurement. It is found that the proposed C2/m structure has enthalpies almost degenerated with those of the *Cmmm* structure over a wide pressure range (40–110 GPa), within which the two structures bear similarities. Upon further compression above 110 GPa, the C2/m structure becomes energetically most stable up to at least 150 GPa. Furthermore, we find that the previously proposed polymeric AlB_2 -type structure does not compete well energetically with *Cmmm* and C2/m phases at these conditions.

To evaluate the dynamical stability and uncover the underlying mechanisms for the stabilization of the C2/m structure, we calculated the phonon dispersion curves for both the

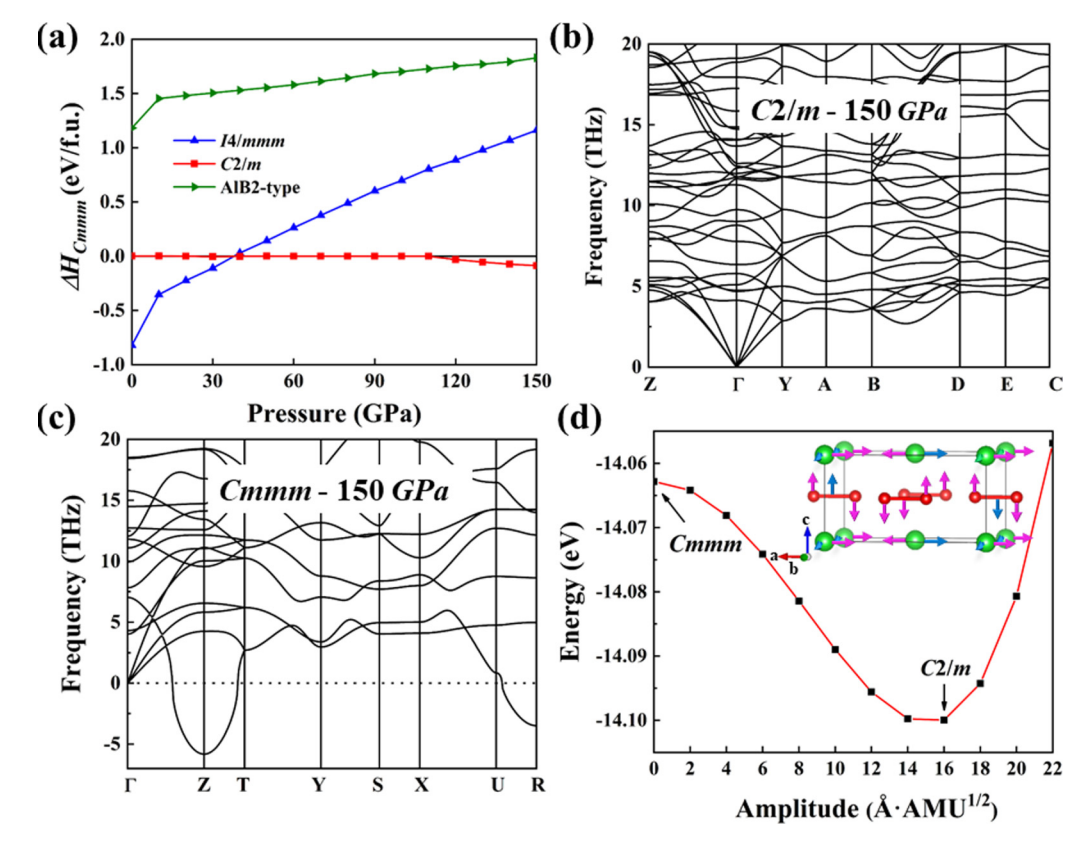


FIG. 2. (a) Enthalpy differences per formula unit as a function of pressure for the I4/mmm, Cmmm, AlB_2 -type, and predicted C2/m structures, where the enthalpies of the Cmmm structure are chosen as the basis. The phonon dispersion curves of (b) C2/m and (c) Cmmm at 150 GPa. (d) Changes in energy as a function of the atom displacement [corresponding to the soft phonon modes both at Z (0.0, 0.0, 0.5) and R (-0.5, 0.5, 0.5) points] with various amplitude values at 150 GPa for the Cmmm structure. Inset shows the atomic motion in the soft phonon modes. The pink and blue arrows represent the atomic vibrational modes at the Z point and the R point of the Cmmm structure, respectively.

216

217

218

219

220

221

222

224

225

226

227

228

230

231

232

233

234

236

237

238

239

240

242

243

244

245

246

248

249

250

251

252

253

254

255

256

257

258

259

260

261

262

263

265

266

267

268

269

271

272

Cmmm and C2/m structure at 150 GPa [Figs. 2(b) and 2(c)]. The C2/m structure is dynamically stable at 150 GPa, as manifested by the absence of imaginary frequencies in the whole Brillouin zone. In contrast, soft phonon modes with imaginary frequency are found at the Z point (0.0, 0.0, 0.5) and the R point (-0.5, 0.5, 0.5) for the Cmmm structure, suggesting a structural instability. The soft phonon modes in the Cmmm structure at 150 GPa are demonstrated in the inset in Fig. 2(d). The mode at the Z point corresponds to vibrations of Ba atoms along a axis and librations of the peroxide groups in the ac plane, while the mode at the R point accounts for vibrations of Ba atoms along the a/b axis and vibrations of part of the peroxide groups in the ac plane.

We further performed frozen-phonon calculations to investigate the structural instability induced by the soft modes in the Cmmm structure; the total energy is calculated as a function of atomic displacements along the eigenvectors of soft modes at both Z and R points, while the rest of the structural parameters are maintained at the values of the parent structure. Note that the atomic displacements are created from the real parts of the eigenvectors representing the amplitudes of vibrations and the phase factors. It is clearly seen from Fig. 2(d) that the total energy curve shows a minimum, indicating the instability of the original Cmmm structure at 150 GPa. Based on the eigenvectors of the two soft modes, we distorted the original Cmmm phase and then minimized the enthalpy by fully optimizing the lattice parameters and atomic positions, which eventually leads to our predicted C2/m structure. This demonstrates that the transition from orthorhombic Cmmm structure to the lower-symmetry C2/m structure is driven by the phonon softening at both the R and Z points.

To provide insights into the phase change at phase transition pressure, we performed synchrotron XRD measurements at various pressures. First, we have performed the XRD measurements on the pressure increase, combining them with Raman probes. Our experiments confirmed the results of Ref. [15] concerning the phase change at 30–50 GPa, where the ambient CaC₂-type phase of BaO₂ transforms reversibly to an orthorhombic phase around 37 GPa [Figs. 3 and 4(a)]. Indeed, XRD measurements showed a drastic change and coexistence of the two phases at 38 GPa (Fig. 3), while the Raman spectra show the O-O band discontinuity in the same pressure range and again the two-phase pressure coexistence range [Fig. 4(a)]. Based on the measurements up to 130 GPa, Cmmm BaO₂ appears to be stable to the highest pressure of our experiments. However, due to the nonhydrostatic stress generated under high pressure, the XRD peak broadening complicates the structural determination. At the highest pressures up to 130 GPa, the sample was laser heated above 2000 K to release stresses and to facilitate possible phase transformation, which otherwise would be hindered because of the existence of the potential barriers between very dissimilar structures. The XRD pattern collected at 96 GPa after the laser heating demonstrated a dramatic narrowing of the XRD peaks that belong to the initial phase along with an appearance of weak single crystal reflections of a second phase [Figs. 3 and S1 in the Supplemental Material [35]]. This impurity phase can be indexed to the MnF₂ distorted fluorite P-42 m structure with the following lattice parameters: a = 4.841(1) and c = 5.127(1) Å, while DFT calculations

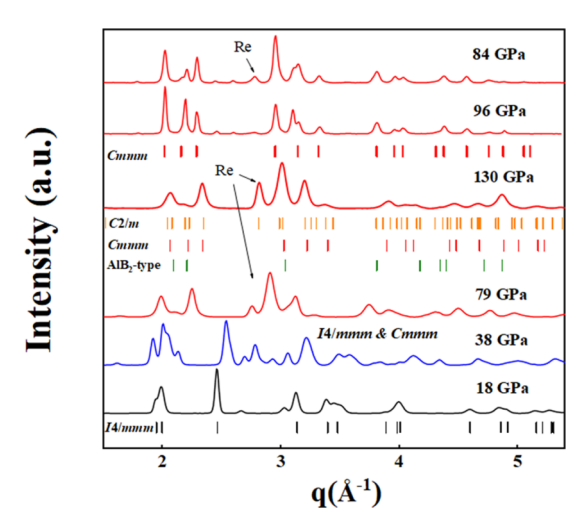


FIG. 3. X-ray diffraction (XRD) patterns measured in the diamond anvil cell experiment of this paper. The data are integrated using DIOPTAS [32], and the background is subtracted. The patterns presented by different colors correspond to different phases. The pressure was increased to 130 GPa at room temperature, and then the sample was laser heated. After this, the pressure dropped to 96 GPa, and XRD patterns were measured on the pressure release. Ticks indicate simulated XRD peaks for different phases, and "Re" denotes the diffraction peak of the rhenium gasket.

show that BaO_2 in this structure is energetically unfavorable. Meanwhile, XRD of the major phase, which shows almost uniform powder rings, can be indexed and refined for both the monoclinic C2/m and orthorhombic Cmmm phases, while a hypothetical polymeric AlB_2 -type phase does not fit well to the experimental data (Fig. 3). The simulated XRD patterns of the C2/m and Cmmm phases are similar (Fig. 3 and S2 in the Supplemental Material [35]): minor splitting of the diffraction peaks and a few very weak additional peaks can be seen in the C2/m phase compared with the Cmmm phase. Therefore, our data do not allow an unambiguous identification of these two structures, thus making it difficult to detect the phase transition by using this technique.

275

278

279

281

289

290

296

297

301

302

305

To unravel this difficulty, we conducted a separate Raman experiment aiming to detect the transition between the C2/mand Cmmm phases. Below 50 GPa, we have been able to reproduce the low-pressure phase transition from I4/mmm to Cmmm reported previously at 34 GPa [15] by observing the Raman peroxide mode doublet in the phase coexistence range at around 37 GPa [Fig. 4(a)]. At higher-pressure range, we followed the higher frequency peak corresponding to Cmmm BaO₂ [Figs. 4(b) and 5(a)]. The results up to \sim 120 GPa show a small kink at ~110 GPa in the pressure dependence of the frequency of the peroxide Raman peak [Fig. 5(a)]. The kink can be observed more clearly from the derivative of the Raman peak position vs pressure, which demonstrates a change in the slope at the proposed transition pressure (Fig. S3 in the Supplemental Material [35]). This observation is like the predicted change of the peak frequency in the theoretical calculation for Cmmm and C2/m Raman spectra [Fig. 5(a)], indicating a possible phase transition at \sim 110 GPa. The persistence of the peroxide Raman band to the highest pressure suggests that no polymerization occurs. As shown in Fig. 4(c),

322

323

324

326

327

329

331

332

FIG. 4. Raman spectra of BaO₂ at various pressures. (a) The Raman spectra of the low-pressure phase transition from I4/mmm to Cmmm. The laser excitation wavelength is $\lambda = 532$ nm. (b) The Raman spectra of BaO₂ at high-pressure range with laser excitation wavelength $\lambda = 632.8$ nm. (c) The comparison of experimental Raman spectrum with theoretical ones for different structures at 120 GPa.

the calculated Raman peak positions for C2/m and Cmmm phases agree with the experiment data, while the Raman peak of the polymeric AlB₂-type phase is not.

307

308

309

310

311

312

313

314

315

317

318

319

Our XRD measurements determined the pressure variations in the crystal volume for BaO_2 in Cmmm phase up to 130 GPa, extending the results of Ref. [15]. The results are presented in Fig. 5(b), which include the results of measurements on the pressure increase before laser heating and on the subsequent pressure release, showing a smooth curve that can be fitted by a single equation of state (EOS). The P(V) data of this paper were fitted together with the data of Ref. [15] for the Cmmm phase to the Rydberg-Vinet EOS [36], which has been found to be one of the most accurate at very high pressure. In addition, it gives a better determination than

previously in Ref. [15] of the two compression parameters: the bulk modulus (B_0) and its pressure derivative (B'_0) . We obtained the following values for the best fitted parameters: $B_0 = 253(07)$ GPa and $B'_0 = 4.18(6)$ with fixed $V_0 = 36 \text{ Å}^3$ (P = 33.6 GPa) that conform to the previous results under low-pressure condition [15]. Moreover, the theoretical P(V) data for *Cmmm* and C2/m phases are also in good agreement with the experiential ones. Since the C2/m phase can be derived by a subtle sublattice distortion of the Ba atom sublattice and rotation of the peroxide groups associated with the phonon mode softening of the lower-pressure *Cmmm* structure, the phase transition is close to a continuous second-order phase transition, where no volume discontinuity is expected.

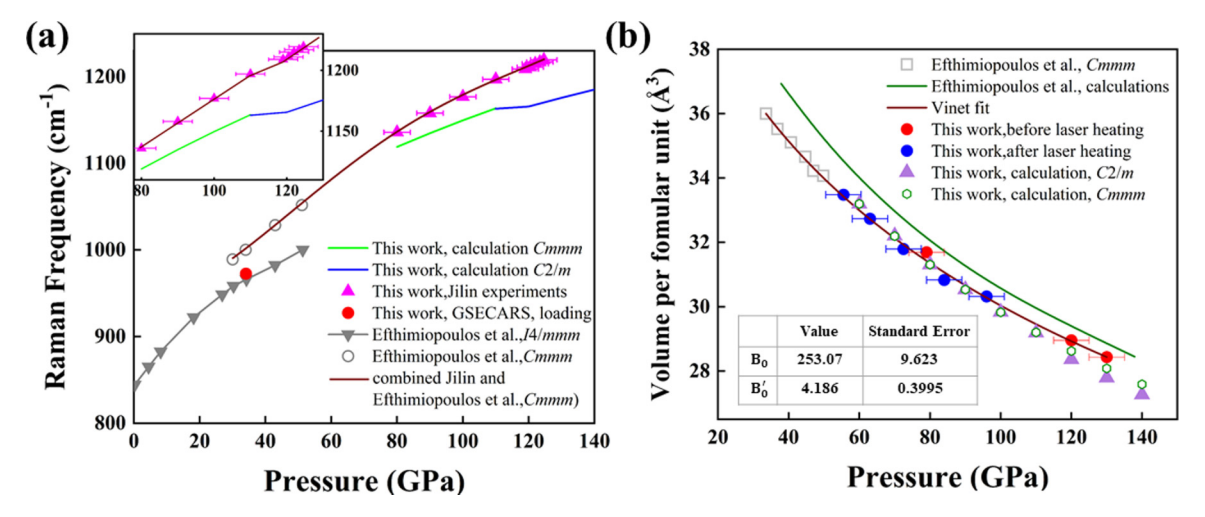


FIG. 5. (a) Frequencies of the measured and calculated Raman modes of BaO₂ as a function of pressure. The solid gray triangles and open gray circles are the data reported in Ref. [15]. Solid green and blue lines are the calculated Raman data of *Cmmm* and C2/m structures, respectively. Inset shows zoomed-in experimental and theoretical dependencies at high pressures. The error bars in the Jilin experiment are indicated when they are smaller or larger than the size of the symbols, and the error bars on the frequencies are smaller than the size of the symbols. (b) Volume per formula unit for the orthorhombic *Cmmm* structure of BaO₂ at high pressure range in comparison with those previously obtained at lower pressure condition. The squares and green solid line are the experimental and calculated data reported in Ref. [15]. The hexagons and solid purple triangles are the calculated volumes of *Cmmm* and C2/m structures, respectively. Red and blue solid circles correspond to data in this paper measured before and after laser heating, respectively. The error bars at each data point are indicated when they are smaller or larger than the size of the symbols. The solid line is the Vinet fit, as given in the text, with $B_0 = 253(07)$ GPa and $B_0' = 4.18(6)$ by fixed $V_0 = 36$ Å³ (P = 33.6 GPa).

372

373

378

379

380

381

382

383

385

391

394

397

400

401

402

403

334

335

336

337

338

340

341

343

346

347

348

349

351

352

353

354

355

357

358

359

360

361

363

364

365

366

367

368

FIG. 6. (a) Electronic band structures (left panel) and projected density of states (right panel) of C2/m structure at 110 GPa. (b) The band gap values of Cmmm and C2/m structures at various pressure.

To provide insights into the electronic properties of the C2/m phase of BaO₂, we calculated the electronic band structures and the corresponding projected density of states at various pressures up to 180 [Figs. 6(a) and S4 in the Supplemental Material [35]]. The results show that the C2/mphase of BaO₂ is insulating in its stability field (above 110 GPa). Due to the charge transfer from Ba atoms to the peroxide O₂ groups, the valence and conduction bands are mainly derived from the O-2 p and Ba-5 d states, respectively. Figure 6(b) shows the variation of band gaps as a function of pressure for the Cmmm and C2/m phases. Interestingly, the band gap gradually decreases in the *Cmmm* phase and then increases upon the transition to the C2/m phase, thus demonstrating the smallest band gap in the Cmmm phase near the phase transition (110 GPa). Under compressions, the decrease of the band gap in the Cmmm phase is a normal phenomenon, as pressure induces an increase in the electron density and electronic kinetic energy that usually results in electronic band broadening and gap closure. After the transition from the Cmmm to the C2/m phase, however, the rearrange of the atoms would lead to enhanced interactions between the Ba atoms and peroxide O₂ groups, which is responsible for the stabilization of the C2/m phase and induces an enlarged band gap.

IV. CONCLUSIONS

In summary, by means of first-principles calculations and CALYPSO structure searches, we identified a monoclinic phase of BaO_2 containing rotated peroxide groups with space group C2/m, which is stable under pressure above 110 GPa. The frozen-phonon calculations indicate that the C2/m structure can be derived by a softening of the Brillouin boundary phonon modes of the low-pressure Cmmm structure. Electronic structure calculations suggest that the C2/m phase is a semiconductor demonstrating an increasing band gap under compression. Although our high-pressure powder XRD measurements cannot definitively select between the lower-

pressure Cmmm and the C2/m structures up to 120 GPa, they clearly rule out the previously proposed oxygen subsystem polymerization. On the other hand, a small but measurable anomaly in the pressure dependence of the peroxide Raman band of barium peroxide at 110 GPa supports the proposed phase transition. Contrary to the previous expectation of polymerization of the peroxide group at elevated pressure, our calculations show that the previously overlooked C2/m phase retains the peroxide group at least up to 130 GPa. The results enrich our understanding of the crystal structures and electronic properties of alkaline earth metal peroxide compounds at high pressure.

ACKNOWLEDGMENTS

The authors acknowledge funding support from the Jilin Province Outstanding Young Talents project (Project No. 20190103040JH), National Natural Science Foundation of China (Grants No. 91961204, No. 11974134, and No. 11534003), the Fundamental Research Funds for the Central Universities (Jilin University, JLU), National Key Research and Development Program of China (under Grant No. 2016YFB0201201), and China Postdoctoral Science Foundation (Grant No. 2017M620107 and No. 2018T110243).

Portions of this paper were performed at GeoSoilEnviroCARS (Secror 13) and HPCAT (Sector 16), Advanced Photon Source (APS), Argonne National Laboratory. HPCAT operations are supported by the Office of Experimental Sciences, US Department of Energy (DOE), National Nuclear Security Administration. GeoSoilEnviroCARS is supported by the National Science Foundation—Earth Sciences (Grant No. EAR—1634415) and Department of Energy GeoSciences (Grant No. DE-FG02-94ER14466). The APS is a DOE Office of Science User Facility operated for the DOE Office of Science by Argonne National Laboratory under Contract No. DE-AC02-06CH11357. At the Earth and Planets Laboratory, we acknowledge the support of the Carnegie Institution of Washington.

^[1] I. Vol'nov and A. W. Petrocelli, *Peroxides, Superoxides, and Ozonides of Alkali and Alkaline Earth Metals* (Springer, Boston, 1966).

^[2] N. G. Vannerberg, Prog. Inorg. Chem. 4, 125 (1962).

^[3] L. J. Quan, B. Zhang, W. W. Shi, and H. Y. Li, J. Integr. Plant Biol. 50, 2 (2008).

- [4] A. D. Bokare and W. Choi, Environ. Sci. Technol. 44, 7232 (2010).
- [5] S. C. Middleburgh, K. P. D. Lagerlof, R. W. Grimes, and W. Y. Ching, J. Am. Ceram. Soc. 96, 308 (2013).
- [6] G. F. Brent and M. D. Harding, Propell. Explos. Pyrot. 20, 300 (1995).
- [7] J. P. Farr, W. L. Smith, and D. S. Steichen, *Kirk-Othmer Encyclopedia of Chemical Technology*, 4th ed. (Wiley, New York, 1992), Vol. 4, p. 271.
- [8] A. J. Carrillo, D. Sastre, D. P. Serrano, P. Pizarro, and J. M. Coronado, Phys. Chem. Chem. Phys. 18, 8039 (2016).
- [9] E. D. J. D. Bernal, I. Kasarnowsky, S. Reichstein, and A. G. Ward, Z. Kristallogr. 92, 344 (1935).
- [10] M. Königstein and C. R. ACatlow, J. Solid State Chem. 140, 103 (1998).
- [11] R. J. F. Berger, M. Hartmann, P. Pyykkö, D. Sundholm, and H. Schmidbaur, Inorg. Chem. 40, 2270 (2001).
- [12] X. Zhao, M. C. Nguyen, C.-Z. Wang, and K.-M. Ho, RSC Adv. 3, 22135 (2013).
- [13] S. S. Lobanov, Q. Zhu, N. Holtgrewe, C. Prescher, V. B. Prakapenka, A. R. Oganov, and A. F. Goncharov, Sci. Rep. 5, 13582 (2015).
- [14] M. Königstein, J. Solid State Chem. 147, 478 (1999).
- [15] I. Efthimiopoulos, K. Kunc, S. Karmakar, K. Syassen, M. Hanfland, and G. Vajenine, Phys. Rev. B 82, 134125 (2010).
- [16] Y. Wang, S. Wang, Y. Zhang, J. Lv, Y. Chen, W. Zheng, and Y. Ma, Inorg. Chem. 56, 7545 (2017).
- [17] J. R. Nelson, R. J. Needs, and C. J. Pickard, Phys. Chem. Chem. Phys. 17, 6889 (2015).
- [18] Y. Wang, J. Lv, L. Zhu, and Y. Ma, Phys. Rev. B 82, 094116 (2010).
- [19] Y. Wang, J. Lv, L. Zhu, and Y. Ma, Comput. Phys. Commun. 183, 2063 (2012).

- [20] J. Lv, Y. Wang, L. Zhu, and Y. Ma, J. Chem. Phys. 137, 084104 (2012).
- [21] B. Gao, P. Gao, S. Lu, J. Lv, Y. Wang, and Y. Ma, Sci. Bull. 64, 301 (2019).
- [22] J. Lv, Y. Wang, L. Zhu, and Y. Ma, Phys. Rev. Lett. 106, 015503 (2011).
- [23] L. Zhu, H. Liu, C. J. Pickard, G. Zou, and Y. Ma, Nat. Chem. 6, 644 (2014).
- [24] X. Feng, X. Zhang, H. Liu, X. Qu, S. A. T. Redfern, J. S. Tse, and Q. Li, RSC Adv. 6, 52695 (2016).
- [25] J. Lv, M. Xu, S. Lin, X. Shao, X. Zhang, Y. Liu, Y. Wang, Z. Chen, and Y. Ma, Nano Energy 51, 489 (2018).
- [26] X. Zhang, W. Zhao, S. Liu, L. Yang, Q. Guo, J. Lv, and Y. Wang, Phys. Rev. B 101, 134112 (2020).
- [27] G. Kresse and J. Furthmüller, Phys. Rev. B **54**, 11169 (1996).
- [28] P. E. Blöchl, Phys. Rev. B 50, 17953 (1994).
- [29] J. P. Perdew, K. Burke, and M. Ernzerhof, Phys. Rev. Lett. 77, 3865 (1996).
- [30] A. Togo and I. Tanaka, Scripta Mater 108, 1 (2015).
- [31] K. Momma and F. Izumi, J. Appl. Crystallogr. 44, 1272 (2011).
- [32] C. Prescher and V. B. Prakapenka, High Pressure Res. 35, 223 (2015).
- [33] N. Holtgrewe, E. Greenberg, C. Prescher, V. B. Prakapenka, and A. F. Goncharov, High Pressure Res. 39, 457 (2019).
- [34] Y. Akahama and H. Kawamura, J. Appl. Phys. 96, 3748 (2004).
- [35] See Supplemental Material at https://link.aps.org/supplemental/ 10.1103/PhysRevB.00.000000 for the experimental and simulated x-ray diffraction (XRD) patterns of the *Cmmm* and *C2/m* phases of BaO₂, the derivatives of the experimental BaO₂ Raman peak positions with respect to pressures, and electronic structures of *C2/m* phase at various pressures.
- [36] P. Vinet, J. R. Smith, J. Ferrante, and J. H. Rose, Phys. Rev. B **35**, 1945 (1987).